



**HAL**  
open science

# Kinetic Monte Carlo Algorithms for Active Matter Systems

Juliane Klamser, Olivier Dauchot, Julien Tailleur

► **To cite this version:**

Juliane Klamser, Olivier Dauchot, Julien Tailleur. Kinetic Monte Carlo Algorithms for Active Matter Systems. *Physical Review Letters*, 2021, 127 (15), pp.150602. 10.1103/PhysRevLett.127.150602 . hal-03840717

**HAL Id: hal-03840717**

**<https://hal.science/hal-03840717v1>**

Submitted on 22 Oct 2024

**HAL** is a multi-disciplinary open access archive for the deposit and dissemination of scientific research documents, whether they are published or not. The documents may come from teaching and research institutions in France or abroad, or from public or private research centers.

L'archive ouverte pluridisciplinaire **HAL**, est destinée au dépôt et à la diffusion de documents scientifiques de niveau recherche, publiés ou non, émanant des établissements d'enseignement et de recherche français ou étrangers, des laboratoires publics ou privés.

# Kinetic Monte Carlo Algorithms for Active Matter systems

Juliane U. Klamsner,<sup>1,\*</sup> Olivier Dauchot,<sup>1,†</sup> and Julien Tailleur<sup>2,‡</sup>

<sup>1</sup>*Gulliver UMR CNRS 7083, ESPCI Paris, Université PSL, 75005 Paris, France*

<sup>2</sup>*Laboratoire Matière et Systèmes Complexes (MSC),  
UMR 7057 CNRS, Université de Paris, 75205 Paris, France*

(Dated: December 30, 2021)

We study kinetic Monte Carlo (KMC) descriptions of active particles. We show that, when they rely on purely persistent, active steps, their continuous-time limit is ill-defined, leading to the vanishing of trademark behaviors of active matter such as the motility-induced phase separation, ratchet effects, as well as to a diverging mechanical pressure. We then show how, under an appropriate scaling, mixing passive steps with active ones leads to a well-defined continuous-time limit that however differs from standard active dynamics. Finally, we propose new KMC algorithms whose continuous-time limits lead to the dynamics of active Ornstein-Uhlenbeck, active Brownian, and run-and-tumble particles.

Monte Carlo (MC) methods are widely popular across disciplines [1, 2]. At equilibrium, detailed balance is enforced and unphysical dynamics can be used while preserving the steady-state Boltzmann distribution. Unphysical tricks can then be exploited to accelerate equilibration without altering steady-state averages of one-time observables, a property which has led to many breakthroughs in equilibrium statistical physics [3–5]. MC algorithms have also been used to study diverse nonequilibrium phenomena like coarsening [6–8], slow relaxation in disordered systems [9–11], granular media [12–15], self-assembly [16], gel electrophoresis of DNA [17], or surface properties [18]. However, the relevance of discrete-time dynamics for nonequilibrium systems is questionable [19–21] since no detailed-balance symmetry enforces a steady-state distribution that is independent from the MC dynamics. This question is particularly relevant in the field of active matter, where MC simulations have been used extensively to simulate the collective dynamics of active particles [22–35].

Active matter constitutes a class of biological and synthetic systems that are driven out of equilibrium at the microscopic scale [36–38]. In their simplest form, they comprise assemblies of particles that dissipate energy to exert self-propelling forces, hence breaking the fluctuation-dissipation relation that would otherwise drive the dynamics of passive colloids towards Boltzmann equilibrium. Active systems have attracted a lot of attention due to their rich phenomenologies, ranging from collective motion [39, 40], to phase separation in the absence of cohesive forces [41], to spatiotemporal chaos at zero Reynolds number [42–44].

The study of active matter systems is, however, challenging because of two important limitations. Theoretically, first, there is no generic expression for the steady-state distribution of active systems and no counterpart to the Boltzmann weight to guide our intuition. Numerically, then, studying the large-scale properties of active systems requires sampling sizes much larger than the particle persistence length. Defined as the typical distance a

particle travels before it forgets its initial orientation, the persistence length often has to be much larger than the particle size for active matter to display its most exciting features. This makes the system sizes to be simulated much larger than for passive systems [34, 35, 45–48].

To address this problem, a natural strategy would be, following the success of MC in equilibrium, to replace the continuous-time setting in which active dynamics are naturally defined by MC dynamics in which time has been coarse grained. Several attempts along these lines have been introduced recently, in particular to study motility-induced phase separation (MIPS) [25, 30], the two-dimensional melting [30, 33, 49], and high-density binary mixtures [26]. All these approaches however suffer from a major drawback: unlike for equilibrium systems, nothing guarantees that these MC dynamics, even in the proper limit, correspond to *bona fide* continuous-time active dynamics.

In this Letter, we bridge this gap by providing a class of active kinetic MC dynamics (AKMC) whose continuous-time limit—which we construct explicitly—is shown to encompass the celebrated run-and-tumble (RT) [50, 51], active Brownian (AB) [52, 53] and active Ornstein-Uhlenbeck (AOU) [54, 55] dynamics. To do so, we start by analyzing the continuous-time limit of AKMC algorithms that have attracted a lot of attention recently [25–27, 30, 33, 49]. We first show numerically and analytically that algorithms relying exclusively on correlated, ‘active’ steps lead to an ill-defined continuous-time limit. We then show how the introduction of a finite fraction of uncorrelated ‘passive’ steps, together with a rescaling of the propulsion speed, leads to a well-defined continuous active dynamics. Importantly, the latter describes a new class of active particles that differ from AB, RT, and AOU particles, notwithstanding [25–27]. We close the Letter by discussing how our AKMC can be modified to lead to RT, AB, and AOU particles hence providing a generic toolbox to simulate active dynamics using AKMCs.

*Active kinetic Monte Carlo dynamics*— We consider a

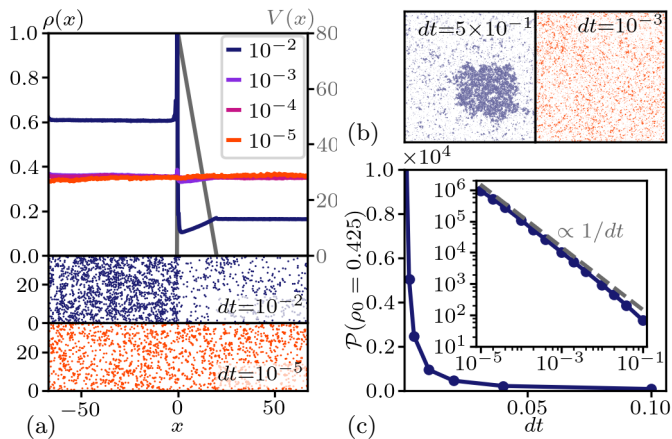


FIG. 1. Simulations of  $N$  interacting active particles in  $2D$  using the AKMC with  $\beta = 1$ . **(a)** As  $dt$  is decreased from  $10^{-2}$  to  $10^{-5}$ , the pumping effect induced by an asymmetric potential  $V(x)$  (solid gray line, upper panel, explicit expression given in SM [56]) disappears, as can be seen by comparing our simulations for  $dt = 10^{-2}$  (snapshot in center panel and density profile shown as blue line in upper panel) and for  $dt = 10^{-5}$  (snapshot in lower panel and density profile shown as red line in upper panel). Parameters:  $\tau = 1$ ,  $v_0 = 4$ , average number density  $\rho_0 \simeq 0.36$ ; periodic (resp. closed) boundary conditions are used along  $y$  (resp.  $x$ ). **(b)** MIPS is observed for  $dt = 0.5$  (blue, left panel) but not for  $dt = 0.001$  (red, right panel), using periodic boundary conditions. Parameters:  $\tau = 200$ ,  $v_0 = 1$ ,  $N = 43\,904$ ,  $L = 468$ . **(c)** The mechanical pressure exerted on a confining potential  $U_w(x, y) = \frac{\Omega}{\nu}(x \pm x_w)^\nu$  for  $|x| > x_w$  is measured using Eq. (2) at bulk number density  $\rho_0 = 0.425$  using periodic boundaries along  $y$ . It diverges as  $1/dt$  when  $dt \rightarrow 0$ . Parameters:  $\tau = 10$ ,  $v_0 = 1$ ,  $L_y = 32$ ,  $x_w = 64$ ,  $\Omega = 10$ ,  $\nu = 8$ .

system of  $N$  active particles endowed with the following dynamics, adapted from [25, 30]. At every time step  $t_n = ndt$ ,  $N$  particles are successively chosen at random and their positions  $\mathbf{r}_i$  and self-propulsion velocities  $\mathbf{v}_i$  are updated, in this order. A particle at  $\mathbf{r}$  moves to a new position  $\mathbf{r} + \mathbf{v}dt$ , with probability

$$f(\mathbf{r}, \mathbf{v}dt) = \min[1, \exp(-\beta\Delta U(\mathbf{r} \rightarrow \mathbf{r} + \mathbf{v}dt))], \quad (1)$$

where  $\beta$  is a control parameter and  $\Delta U = U(\mathbf{r} + \mathbf{v}dt) - U(\mathbf{r})$  is the total energy change. Equation (1) is nothing but a standard equilibrium Metropolis filter, in the context of which  $\beta$  would be the inverse temperature, and the breakdown of detailed balance comes from the dynamics of  $\mathbf{v}$ . A new velocity  $\mathbf{v}(t_{n+1})$  is sampled from a Gaussian distribution centered at  $\mathbf{v}(t_n)$ , of standard deviation  $\delta v = \sqrt{2D_v dt}$ , which is then folded back using reflecting boundary conditions at  $|\mathbf{v}| = v_0$ . (See Fig. S1 in [56] for an illustration of this procedure.) Successive particle displacements are thus correlated, hence leading to a persistent motion characterized, in two space dimensions, by a persistence time  $\tau = \frac{v_0^2}{c^2 D_v}$  where  $c$  is a constant that can be computed exactly (see SM [56]).

Figure 1 shows AKMC simulations of  $N$  particles inter-

acting via a Weeks-Chandler-Andersen potential  $U(r) = 4[(\sigma/r)^{12} - (\sigma/r)^6] + 1$  for  $r < 2^{1/6}\sigma$  and  $U(r) = 0$  otherwise, with  $\sigma = 2^{-1/6}$ . Simulations are shown for different time steps  $dt$ , keeping the self-propulsion speed  $v_0$  and persistence time  $\tau$  constant. Using large time steps, the simulations reproduce standard features of active systems: motility-induced phase separation [41] is observed and asymmetric obstacles are able to pump particles, hence generating long-ranged perturbations to the density field [57–59]. However, both features disappear for smaller time steps. Even more surprising, the mechanical pressure exerted by the particles on a confining potential  $U_w$ , measured as [60]

$$\mathcal{P} = \int_{x_{\text{bulk}}}^{\infty} \rho(x) \partial_x U_w(x), \quad (2)$$

is shown to diverge when  $dt \rightarrow 0$ . The AKMC algorithm introduced in this section is thus not suitable to describe active dynamics.

*Vanishing mobility in the continuous-time limit*— This pathological behavior can be understood analytically by showing that the particle mobility vanishes as  $dt \rightarrow 0$ , making the particles less and less sensitive to forces other than the self-propulsion ones. Let us consider the simpler problem of an isolated particle in the presence of an external potential  $U(x)$  in one space dimension. The generalization to higher dimensions and interacting particles is straightforward. Reformulating the AKMC in one dimension leads to a persistence time  $\tau = 4v_0^2/(\pi^2 D_v)$  [56]. We denote  $P_n(x, v)$  the probability density to find the particle at position  $x$  with velocity  $v$  at time  $t_n$ . Its evolution is given by

$$P_{n+1}(x, v) = \int dx' dv' g(v|v') W(x|x', dt v') P_n(x', v') \quad (3)$$

where  $g(v|v')$  is the probability density to transition from self-propulsion velocity  $v'$  to  $v$  and where

$$W(x|x', \Delta x) \equiv f(x', \Delta x) \delta(x' + \Delta x - x) + [1 - f(x', \Delta x)] \delta(x' - x) \quad (4)$$

is the probability density to transition from  $x'$  to  $x$ . The two terms on the rhs of Eq. (4) correspond to hopping from  $x' \neq x$  into  $x$  and to staying in  $x'$ , respectively.

The continuous-time limit of the evolution equation is obtained by truncating the Kramers-Moyal expansion of  $\Delta P \equiv P_{n+1}(x, v) - P_n(x, v)$  to first order in  $dt$  [61, 62]. This has been done with success for equilibrium MC dynamics—see e.g. [19, 20, 63], or [64] for a nice application to neural networks. As we show in the following, the generalization of this approach to the active case leads to the Fokker-Planck equation [65]:

$$\partial_t P(x, v; t) = -\frac{\partial}{\partial x} [vP(x, v; t)] + D_v \frac{\partial^2}{\partial v^2} P(x, v; t), \quad (5)$$

which is complemented by a zero-current condition

$$\partial_v P(x, v; t)|_{v=\pm v_0} = 0. \quad (6)$$

The main lesson of this calculation is that the confining potential drops out from Eq. (5). To understand better how this happens, it is insightful to write  $\Delta P$  as

$$\begin{aligned} \Delta P &= \int dv' g(v|v') [f(x - v' dt, v' dt) P_n(x - v' dt, v') \\ &\quad - f(x, v' dt) P_n(x, v')] \\ &\quad + \int dv' g(v|v') P_n(x, v') - P_n(x, v). \end{aligned} \quad (7)$$

Consider first the last line of Eq. (7). Taylor expanding  $P_n(x, v')$  close to  $v' = v$  leads to

$$\int dv' g(v|v') P_n(x, v') - P_n(x, v) = \sum_{k>0} \frac{a_k}{k!} \partial_v^k P_n(x, v),$$

where  $a_k$  is related to the  $k^{\text{th}}$  moment of the change in velocity through  $a_k = (-1)^k \int dv' g(v|v') (v - v')^k$ . The coefficient  $a_1$  vanishes by symmetry in the  $dt \rightarrow 0$  limit and  $a_2 = \delta v^2$  provides the dominant order to  $\Delta P$ . This confirms the scaling  $\delta v = \sqrt{2dtD}$ , chosen above and leads to the Laplacian on  $v$  in Eq. (5). The zero-flux condition on  $v$  is simply inherited from that of the discrete-time process [61]. Consider now the first two lines of Eq. (7). To leading order in  $dt$ , they are equivalent to  $-dt \int dv' g(v|v') v' \partial_x [f(x, v' dt) P_n(x, v')]$ . This is already of order  $dt$  so that only the  $\mathcal{O}(1)$  contribution of the integral survives. To estimate the latter, we first note that  $\Delta U \simeq v dt U'(x)$  so that the Metropolis filter can be approximated as  $f(x, v dt) \simeq 1 - \beta v dt U'(x) \frac{1 + \text{sgn}(\Delta U)}{2}$ . To leading order,  $f = 1$  and the AKMC is insensitive to the filter in the continuous-time limit. The computation can then be concluded by using that  $v' = (v' - v) + v$  and Taylor expanding  $P(x, v')$  at  $v' = v$ , yielding a leading order contribution  $-dt v \partial_x P(x, v)$ . Mathematically,  $U$  thus only enters Eq. (5) at the next order in  $dt$ : the mobility of this AKMC vanishes linearly in  $dt$ . Physically,  $U$  is ignored by the particles since a succession of infinitely small persistent steps lead to their systematic acceptance.

The derivation above explains both the uniform distribution measured in Fig. 1a and the suppression of MIPS in Fig. 1b. Furthermore, as  $dt \rightarrow 0$ , particles penetrate more and more into confining walls, so that the mechanical pressure exerted on the walls, measured as Eq. (2), diverges.

*A blended AKMC*— Since KMC algorithms admit a well-defined continuous-time limit in equilibrium [19–21, 63, 64], it is natural to try and interpolate between passive and active KMC dynamics [25]. To do so, we introduce a blended AKMC as follows. At every time step, an attempt to move from  $x$  to  $x + v dt/\alpha$  is done with probability  $\alpha$  whereas a move from  $x$  to  $x + \xi$

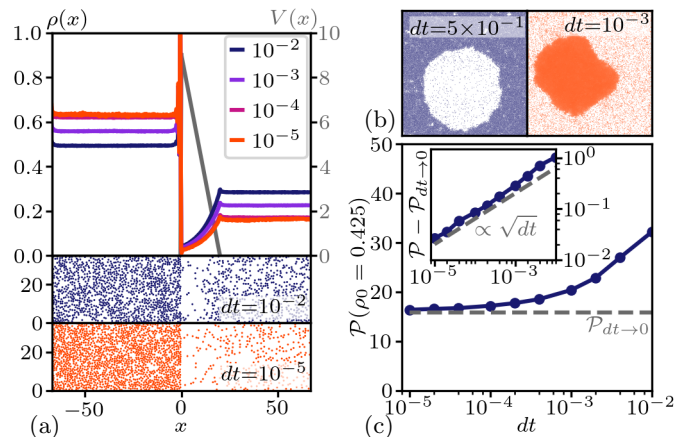


FIG. 2. Simulations of  $N$  interacting active particles using the blended AKMC with  $\beta = 1$  and  $\alpha \in (0, 1)$ . **(a)** As  $dt$  is decreased from  $10^{-2}$  to  $10^{-5}$ , the pumping effect induced by an asymmetric potential  $V(x)$  (gray line, upper panel, explicit expression given in SM [56]) is now converging to a stable nonequilibrium steady state. Parameters:  $\alpha = 0.4$ ,  $\tau = 1$ ,  $v_0 = 4$ ,  $D = 1$ ,  $\rho_0 \simeq 0.36$ . Periodic (resp. closed) boundary conditions are implemented along  $y$  (resp.  $x$ ). **(b)** MIPS is now observed both for  $dt = 0.5$  (blue, left panel) and  $dt = 0.001$  (red, right panel), using periodic boundary conditions. Parameters:  $\alpha = 0.6$ ,  $\tau = 200$ ,  $v_0 = 1$ ,  $D = 0.05$ ,  $N = 43\,904$ ,  $L = 270$ . **(c)** The mechanical pressure exerted on the confining potential  $U_w$  is measured using Eq. (2) and has now a well-defined limit as  $dt \rightarrow 0$ . Parameters:  $\alpha = 0.6$ ,  $\tau = 10$ ,  $v_0 = 1$ ,  $D = 0.05$ . The same geometry, wall potential, and densities are used as in Fig. 1(c).

is attempted with probability  $1 - \alpha$ , where  $\xi$  is sampled uniformly and independently at each time step in  $[-\sqrt{6Ddt/(1-\alpha)}, \sqrt{6Ddt/(1-\alpha)}]$ . In both cases, the move is accepted or rejected using the Metropolis filter defined in (1). Note that the rescaling of the propulsion speed and of the passive diffusivities with  $\alpha$  will be proved below to be crucial to the existence of an  $\alpha$ -independent well-defined continuous-time limit. Figure 2 shows simulation results for  $\alpha = 0.4$  and  $\alpha = 0.6$ . Motility-induced phase separation and a long-range modulation of the density field by an asymmetric obstacle are again observed for large  $dt$ . This time, however, these phenomena are stable as  $dt \rightarrow 0$ . The mechanical pressure exerted on confining walls also admits a well-defined limit.

The continuous-time limit of the blended AKMC can be constructed analytically from the following extension of our calculation. The master equation now writes

$$\begin{aligned} P_{n+1}(x, v) &= \alpha \int dx' dv' g(v|v') W\left(x \left| x', \frac{v' dt}{\alpha} \right.\right) P_n(x', v') \\ &\quad + (1 - \alpha) \int dx' dv' d\xi g(v|v') W(x|x', \xi) P_n(x', v') G(\xi), \end{aligned} \quad (8)$$

where  $G(\xi)$  is the uniform measure over  $[-\sqrt{6Ddt/(1-\alpha)}, \sqrt{6Ddt/(1-\alpha)}]$ . By linearity, the continuous-time limit of this blended AKMC is now readily obtained. The first line of Eq. (8) again leads to

the drift and diffusion terms derived in Eq. (5), albeit the latter multiplied by  $\alpha$ . The second line still leads to the diffusion of the self-propulsion velocity multiplied by  $(1 - \alpha)$ , but also to the standard terms entering the Fokker-Planck equation of a passive particle. All in all, this leads to the Fokker-Planck equation

$$\partial_t P_t(x, v) = -\partial_x [\{v + \mu F(x)\} P_t(x, v)] + D \partial_x^2 P_t(x, v) + D_v \partial_v^2 P_t(x, v) \quad (9)$$

where Eq. (9) is again supplemented by the zero-current condition in Eq. (6). This time, the confining force  $F(x) = -\partial_x U(x)$  survives in the  $dt \rightarrow 0$  limit thanks to a finite mobility  $\mu = \beta D$ . Interestingly, comparing Eqs. (5) and (9) shows that the role played by the passive steps to restore the continuous-time limit is not so much the introduction of translational diffusion as the restoration of a finite mobility.

We now compute the mechanical pressure predicted by Eq. (9) to check that the latter quantitatively describes the small  $dt$  limit of the blended AKMC. Integrating over  $v$  and using the zero-flux condition along  $x$  imposed by the confining wall leads to  $\rho(x)U'_w(x) = -\frac{D}{\mu}\rho'(x) + \frac{1}{\mu}\bar{v}_1(x)$ , where we define  $\bar{v}_k(x) = \int dv P(x, v)v^k$  and  $\rho(x) = \bar{v}_0(x)$ . Further integrating from  $x = 0$  to  $x = \infty$  leads to  $\mathcal{P} = \frac{D}{\mu}\rho_0 + \frac{1}{\mu}\int_0^\infty \bar{v}_1(x)dx$ . To compute the last integral, we multiply Eq. (9) by  $v^k$  and integrate over  $v$  to get, in the steady state,

$$(k-1)\bar{v}_{k-2} = v_0^{k-1}[P(x, v_0) + (-1)^k P(x, -v_0)] + \partial_x \frac{J_k}{kD_v}, \quad (10)$$

where  $J_k \equiv \bar{v}_{k+1} - \bar{v}_k \mu U'_w(x) - D \partial_x \bar{v}_k$ . For  $k = 1$ , Eq. (10) leads to  $[P(x, v_0) - P(x, -v_0)] = -\partial_x J_1 / D_v$ . Injecting this into Eq. (10) for  $k = 3$  and integrating both sides of the equation from  $x = 0$  to  $\infty$  leads to  $6D_v \int_0^\infty \bar{v}_1 dx = [3v_0^2 \bar{v}_2(0) - \bar{v}_4(0)]$ . Since the bulk of the system is homogeneous and isotropic,  $P(x = 0, v) = \rho_0 / (2v_0)$  and the mechanical pressure reads

$$\mathcal{P} = \rho_0 \left( k_B T + \frac{2v_0^4}{15\mu D_v} \right), \quad (11)$$

where we have introduced  $k_B T \equiv \beta^{-1}$ . Figure 3a shows the perfect match between Eq. (11) and the mechanical pressure measured in numerical simulations for five different potential stiffnesses and several values of  $\alpha \in (0, 1)$ . For  $\alpha < 1$ , the pressure does not depend on the potential, which indicates that the blended AKMC satisfies an equation of state in the continuous-time limit. Note that the dependencies on  $\alpha$  of the active steps,  $\mathbf{r} \rightarrow \mathbf{r} + \mathbf{v}dt/\alpha$ , and of the amplitude of the passive ones,  $\xi \in [-\sqrt{6Ddt}/(1-\alpha), \sqrt{6Ddt}/(1-\alpha)]$ , may look surprising at first glance—they were indeed absent in previous AKMCs [25, 30]. They are, however, crucial to lead to continuous-time limits independent of  $\alpha$ , as shown from Eq. (9) and illustrated in Fig. 3.

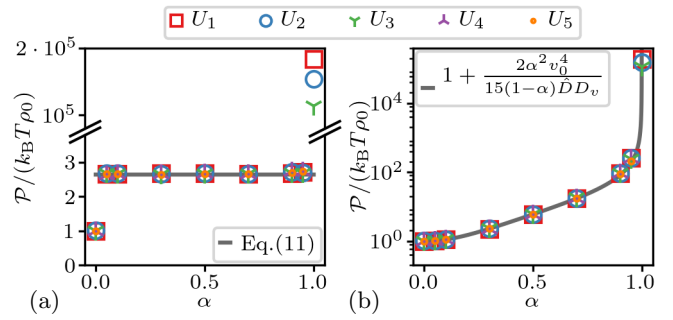


FIG. 3. Mechanical pressure  $\mathcal{P}$ , defined in Eq. (2) and normalized by its equilibrium value  $\mathcal{P} = \rho_0 k_B T$ , measured as a function of the fraction of active steps  $\alpha$  for noninteracting particles in 1d, with  $\beta = 1$ ,  $v_0 = 1$ ,  $\tau = 5$ ,  $dt = 10^{-4}$ . Symbols are measurements for several confining potentials  $U_i$  to  $U_5$ , corresponding to the potential  $U_w$  defined in Fig. 1 with  $(\nu, \Omega)$  given by  $\{(8, 10), (6, 10), (4, 10), (2, 100), (2, 10)\}$ , respectively. The confining walls are located at  $\pm x_w$ . (a) Simulations carried out with the blended AKMC for  $\alpha \in (0, 1)$ ,  $D = 1$ , and  $x_w = 15$ . The limiting cases  $\alpha = 0$  and  $\alpha = 1$  correspond to purely passive and purely active KMCs, respectively. The solid gray line is the prediction of Eq. (11). (b) Simulations carried out without rescaling the active steps and the passive diffusivity, using instead  $x(t_{n+1}) \rightarrow x(t_n) + vdt$  and  $\xi \in [-\sqrt{6\hat{D}dt}, \sqrt{6\hat{D}dt}]$ , where  $\hat{D} = 1/6$  and  $x_w = 5$ . The lack of rescaling leads to an unphysical dependency of the pressure on  $\alpha$ .

*AB, RT, and AOU algorithms.* We have shown that our blended AKMC leads to the Fokker-Planck equation (9) in the continuous-time limit. In two space dimensions, this active dynamics is equivalent to the Langevin equation

$$\dot{\mathbf{r}} = \mathbf{v} - \mu \nabla U(\mathbf{r}) + \sqrt{2D} \boldsymbol{\eta}; \quad \dot{\mathbf{v}} = \sqrt{2D_v} \boldsymbol{\zeta} \quad (12)$$

where  $\boldsymbol{\eta}$  and  $\boldsymbol{\zeta}$  are two uncorrelated unitary Gaussian white noises and  $\mathbf{v}$  experiences reflecting boundary conditions at  $|\mathbf{v}| = v_0$ . Interestingly, the dynamics of  $\mathbf{v}$  corresponds to none of the standard active particle models. As we now show, our blended AKMC can be adapted to yield discrete-time versions of AB, RT and AOU particles by solely modifying the dynamics of the self-propulsion speed. For RT and AB dynamics, the self-propulsion speed  $\mathbf{v}(t_n)$  lives on a circle of radius  $v_0$  and is parametrized by an angle  $\theta(t_n)$ . A discretized RT dynamics with tumbling rate  $\gamma$  is obtained by choosing  $\theta(t_{n+1}) = \theta(t_n)$  with probability  $(1 - \gamma dt)$  and by sampling  $\theta(t_{n+1})$  uniformly in  $[0, 2\pi)$  with probability  $\gamma dt$ . To implement an AB dynamics with rotational diffusivity  $D_r$ ,  $\theta(t_{n+1})$  is sampled from a wrapped Gaussian distribution of standard deviation  $\delta\theta = \sqrt{2D_r dt}$ , centered at  $\theta(t_n)$ . Finally, the AOU dynamics can be implemented as follows. A change of velocity  $\delta\mathbf{v}(t_n)$  is sampled uniformly in  $[-\sqrt{6D_a dt}/(\tau^2), \sqrt{6D_a dt}/(\tau^2)]^2$ . It is accepted when

probability

$$p = \min \left[ 1, \exp \left( - \frac{\tau^2}{D_a} \Delta U_v[\mathbf{v}(t_n) \rightarrow \mathbf{v}(t_n) + \delta\mathbf{v}(t_n)] \right) \right] \quad (13)$$

where  $U_v(\mathbf{v}) = \frac{1}{2\tau} \mathbf{v}^2$ . Carrying out the continuous-time limit of the dynamics indeed leads to the Fokker-Planck equation equivalent to  $\dot{\mathbf{r}} = \mathbf{v} + \mu\mathbf{F} + \sqrt{2D}\boldsymbol{\eta}$  and  $\tau\dot{\mathbf{v}} = -\mathbf{v} + \sqrt{2D_a}\boldsymbol{\zeta}$  where  $\boldsymbol{\eta}$  and  $\boldsymbol{\zeta}$  are two uncorrelated unitary Gaussian white noises.

Altogether we have shown how mixing passive steps with active ones endow AKMCs with *bona fide* continuous-time limits which encompass the workhorse models of active matter. By clarifying the connection between discrete and continuous-time dynamics, we believe our work will trigger a wider use of AKMCs in active matter. They should prove especially useful in the high density limit where Langevin equations are particularly difficult to use. This regime has indeed attracted a lot of attention recently [66–69], in particular due to its relevance to the modeling of confluent tissues [70–72], but also because of the emergence of nontrivial spatial velocity correlations [73–75]. Finally, it would be interesting to generalize the approach developed in this Letter to MC algorithms in which space has also been discretized, which have recently attracted a lot of attention [22–24, 28, 29, 31, 32, 34].

JT acknowledges the financial support of ANR Grant THEMA. The authors benefited from participation in the 2020 KITP program on Active Matter supported by the Grant NSF PHY-1748958.

---

\* juliane.klamser@espci.psl.eu

† olivier.dauchot@espci.fr

‡ julien.tailleur@u-paris.fr

- [1] D. Landau and K. Binder, *A Guide to Monte Carlo Simulations in Statistical Physics* (Cambridge University Press, 2014).
- [2] C. P. Robert and G. Casella, *Monte Carlo statistical methods*. (Springer-Verlag, New York, 2004).
- [3] U. Wolff, Collective monte carlo updating for spin systems, *Phys. Rev. Lett.* **62**, 361 (1989).
- [4] L. Berthier, E. Flenner, C. J. Fullerton, C. Scalliet, and M. Singh, Efficient swap algorithms for molecular dynamics simulations of equilibrium supercooled liquids, *J. Stat. Mech. Theor. Exp.* **2019**, 064004 (2019).
- [5] E. P. Bernard and W. Krauth, Two-step melting in two dimensions: First-order liquid-hexatic transition, *Phys. Rev. Lett.* **107**, 155704 (2011).
- [6] R. J. Glauber, Time-dependent statistics of the ising model, *J. Math. Phys.* **4**, 294 (1963).
- [7] W. K. Hastings, Monte carlo sampling methods using markov chains and their applications, *Biometrika* **57**, 97 (1970).
- [8] P. Peskun, Guidelines for choosing the transition matrix in monte carlo methods using markov chains, *J. Comput. Phys.* **40**, 327 (1981).
- [9] L. Berthier and W. Kob, The monte carlo dynamics of a binary lennard-jones glass-forming mixture, *J. Phys. Condens. Matter* **19**, 205130 (2007).
- [10] L. Berthier and G. Biroli, Theoretical perspective on the glass transition and amorphous materials, *Rev. Mod. Phys.* **83**, 587 (2011).
- [11] A. Ninarello, L. Berthier, and D. Coslovich, Models and algorithms for the next generation of glass transition studies, *Phys. Rev. X* **7**, 021039 (2017).
- [12] M. Müller and H. J. Herrmann, Dsmc — a stochastic algorithm for granular matter, in *Physics of Dry Granular Media*, edited by H. J. Herrmann, J.-P. Hovi, and S. Luding (Springer Netherlands, Dordrecht, 1998) pp. 413–420.
- [13] J. J. Brey and M. Ruiz-Montero, Direct monte carlo simulation of dilute granular flow, *Computer physics communications* **121**, 278 (1999).
- [14] J. M. Montanero and A. Santos, Computer simulation of uniformly heated granular fluids, *Granular Matter* **2**, 53 (2000).
- [15] M. A. Cárdenas-Barrantes, J. D. Muñoz, and W. F. Oquendo, Contact forces distribution for a granular material from a monte carlo study on a single grain, *Granular Matter* **20**, 1 (2018).
- [16] G. Bisker and J. L. England, Nonequilibrium associative retrieval of multiple stored self-assembly targets, *Proceedings of the National Academy of Sciences* **115**, E10531 (2018).
- [17] G. Barkema and M. Newman, The repton model of gel electrophoresis, *Physica A* **244**, 25 (1997).
- [18] M. Breeman, G. Barkema, M. Langelaar, and D. Boerma, Computer simulation of metal-on-metal epitaxy, *Thin Solid Films* **272**, 195 (1996).
- [19] E. Sanz and D. Marenduzzo, Dynamic monte carlo versus brownian dynamics: A comparison for self-diffusion and crystallization in colloidal fluids, *J. Chem. Phys.* **132**, 194102 (2010).
- [20] S. Jabbari-Farouji and E. Trizac, Dynamic monte carlo simulations of anisotropic colloids, *J. Chem. Phys.* **137**, 054107 (2012).
- [21] M. E. J. Newman and G. T. Barkema, *Monte Carlo Methods in Statistical Physics* (Oxford University Press, 1999).
- [22] F. Peruani, T. Klaus, A. Deutsch, and A. Voss-Boehme, Traffic jams, gliders, and bands in the quest for collective motion of self-propelled particles, *Phys. Rev. Lett.* **106**, 128101 (2011).
- [23] A. G. Thompson, J. Tailleur, M. E. Cates, and R. A. Blythe, Lattice models of nonequilibrium bacterial dynamics, *J. Stat. Mech. Theor. Exp.* **2011**, P02029 (2011).
- [24] R. Soto and R. Golestanian, Self-assembly of catalytically active colloidal molecules: Tailoring activity through surface chemistry, *Phys. Rev. Lett.* **112**, 068301 (2014).
- [25] D. Levis and L. Berthier, Clustering and heterogeneous dynamics in a kinetic monte carlo model of self-propelled hard disks, *Phys. Rev. E* **89**, 062301 (2014).
- [26] L. Berthier, Nonequilibrium glassy dynamics of self-propelled hard disks, *Phys. Rev. Lett.* **112**, 220602 (2014).
- [27] D. Levis and L. Berthier, From single-particle to collective effective temperatures in an active fluid of self-propelled particles, *EPL* **111**, 60006 (2015).
- [28] N. Sepúlveda and R. Soto, Coarsening and clustering in run-and-tumble dynamics with short-range exclusion,

- Phys. Rev. E **94**, 022603 (2016).
- [29] A. Manacorda and A. Puglisi, Lattice model to derive the fluctuating hydrodynamics of active particles with inertia, Phys. Rev. Lett. **119**, 208003 (2017).
- [30] J. U. Klamsner, S. C. Kapfer, and W. Krauth, Thermodynamic phases in two-dimensional active matter, Nat Commun. **9**, 5045 (2018).
- [31] S. Whitelam, K. Klymko, and D. Mandal, Phase separation and large deviations of lattice active matter, J. Chem. Phys. **148**, 154902 (2018).
- [32] M. Kourbane-Houssene, C. Erignoux, T. Bodineau, and J. Tailleur, Exact hydrodynamic description of active lattice gases, Phys. Rev. Lett. **120**, 268003 (2018).
- [33] J. U. Klamsner, S. C. Kapfer, and W. Krauth, A kinetic-monte carlo perspective on active matter, J. Chem. Phys. **150**, 144113 (2019).
- [34] X.-q. Shi, G. Fausti, H. Chaté, C. Nardini, and A. Solon, Self-organized critical coexistence phase in repulsive active particles, Phys. Rev. Lett. **125**, 168001 (2020).
- [35] S. Ro, Y. Kafri, M. Kardar, and J. Tailleur, Disorder-induced long-ranged correlations in scalar active matter, Phys. Rev. Lett. **126**, 048003 (2021).
- [36] M. C. Marchetti, J.-F. Joanny, S. Ramaswamy, T. B. Liverpool, J. Prost, M. Rao, and R. A. Simha, Hydrodynamics of soft active matter, Rev. Mod. Phys. **85**, 1143 (2013).
- [37] C. Bechinger, R. Di Leonardo, H. Löwen, C. Reichhardt, G. Volpe, and G. Volpe, Active particles in complex and crowded environments, Rev. Mod. Phys. **88**, 045006 (2016).
- [38] P. Romanczuk, M. Bär, W. Ebeling, B. Lindner, and L. Schimansky-Geier, Active brownian particles, The European Physical Journal Special Topics **202**, 1 (2012).
- [39] T. Vicsek and A. Zafeiris, Collective motion, Phys. Rep. **517**, 71 (2012).
- [40] H. Chaté, Dry aligning dilute active matter, Annual Review of Condensed Matter Physics **11**, 189 (2020).
- [41] M. E. Cates and J. Tailleur, Motility-induced phase separation, Annu. Rev. Condens. Matter Phys. **6**, 219 (2015).
- [42] H. H. Wensink, J. Dunkel, S. Heidenreich, K. Drescher, R. E. Goldstein, H. Löwen, and J. M. Yeomans, Mesoscale turbulence in living fluids, Proceedings of the National Academy of Sciences **109**, 14308 (2012).
- [43] J. Stenhammar, C. Nardini, R. W. Nash, D. Marenduzzo, and A. Morozov, Role of correlations in the collective behavior of microswimmer suspensions, Phys. Rev. Lett. **119**, 028005 (2017).
- [44] K.-T. Wu, J. B. Hishamunda, D. T. Chen, S. J. DeCamp, Y.-W. Chang, A. Fernández-Nieves, S. Fraden, and Z. Dogic, Transition from turbulent to coherent flows in confined three-dimensional active fluids, **355**, eaal1979 (2017).
- [45] G. Grégoire and H. Chaté, Onset of collective and cohesive motion, Phys. Rev. Lett. **92**, 025702 (2004).
- [46] C. A. Weber, T. Hanke, J. Deseigne, S. Léonard, O. Dauchot, E. Frey, and H. Chaté, Long-range ordering of vibrated polar disks, Phys. Rev. Lett. **110**, 208001 (2013).
- [47] A. Solon and J. Tailleur, Revisiting the flocking transition using active spins, Phys. Rev. Lett. **111**, 078101 (2013).
- [48] A. P. Solon, H. Chaté, and J. Tailleur, From phase to microphase separation in flocking models: The essential role of nonequilibrium fluctuations, Phys. Rev. Lett. **114**, 068101 (2015).
- [49] P. Digregorio, D. Levis, A. Suma, L. F. Cugliandolo, G. Gonnella, and I. Pagonabarraga, Full phase diagram of active brownian disks: From melting to motility-induced phase separation, Phys. Rev. Lett. **121**, 098003 (2018).
- [50] M. J. Schnitzer, Theory of continuum random walks and application to chemotaxis, Physical Review E **48**, 2553 (1993).
- [51] H. C. Berg, *E. coli in Motion* (Springer Science & Business Media, 2008).
- [52] Y. Fily and M. C. Marchetti, Athermal phase separation of self-propelled particles with no alignment, Phys. Rev. Lett. **108**, 235702 (2012).
- [53] T. F. Farage, P. Krinninger, and J. M. Brader, Effective interactions in active brownian suspensions, Physical Review E **91**, 042310 (2015).
- [54] G. Szamel, Self-propelled particle in an external potential: Existence of an effective temperature, Physical Review E **90**, 012111 (2014).
- [55] D. Martin, J. O’Byrne, M. E. Cates, É. Fodor, C. Nardini, J. Tailleur, and F. van Wijland, Statistical mechanics of active ornstein-uhlenbeck particles, Physical Review E **103**, 032607 (2021).
- [56] See Supplemental Material [url] which includes numerical details.
- [57] P. Galajda, J. Keymer, P. Chaikin, and R. Austin, A wall of funnels concentrates swimming bacteria, Journal of bacteriology **189**, 8704 (2007).
- [58] M. Wan, C. O. Reichhardt, Z. Nussinov, and C. Reichhardt, Rectification of swimming bacteria and self-driven particle systems by arrays of asymmetric barriers, Phys. Rev. Lett. **101**, 018102 (2008).
- [59] J. Tailleur and M. Cates, Sedimentation, trapping, and rectification of dilute bacteria, EPL (Europhysics Letters) **86**, 60002 (2009).
- [60] A. P. Solon, Y. Fily, A. Baskaran, M. E. Cates, Y. Kafri, M. Kardar, and J. Tailleur, Pressure is not a state function for generic active fluids, Nat. Phys. **11**, 673 (2015).
- [61] C. W. Gardiner *et al.*, *Handbook of stochastic methods*, Vol. 3 (springer Berlin, 1985).
- [62] N. G. Van Kampen, *Stochastic processes in physics and chemistry*, Vol. 1 (Elsevier, 1992).
- [63] K. Kikuchi, M. Yoshida, T. Maekawa, and H. Watanabe, Metropolis monte carlo method as a numerical technique to solve the fokker—planck equation, Chem. Phys. Lett. **185**, 335 (1991).
- [64] S. Whitelam, V. Selin, S.-W. Park, and I. Tambllyn, Correspondence between neuroevolution and gradient descent (2021), arXiv:2008.06643 [cs.NE].
- [65] J. Klamsner, O. Dauchot, J. Tailleur, in preparation.
- [66] S. Henkes, Y. Fily, and M. C. Marchetti, Active jamming: Self-propelled soft particles at high density, Physical Review E **84**, 040301(R) (2011).
- [67] E. Flenner, G. Szamel, and L. Berthier, The nonequilibrium glassy dynamics of self-propelled particles, Soft matter **12**, 7136 (2016).
- [68] L. Berthier, E. Flenner, and G. Szamel, Glassy dynamics in dense systems of active particles, The Journal of chemical physics **150**, 200901 (2019).
- [69] R. Mandal, P. J. Bhuyan, P. Chaudhuri, C. Dasgupta, and M. Rao, Extreme active matter at high densities, Nat. Commun. **11**, 2581 (2020).
- [70] D. Matoz-Fernandez, K. Martens, R. Sknepnek, J. Barrat, and S. Henkes, Cell division and death inhibit glassy behaviour of confluent tissues, Soft matter **13**, 3205

- (2017).
- [71] B. Loewe, M. Chiang, D. Marenduzzo, and M. C. Marchetti, Solid-liquid transition of deformable and overlapping active particles, *Phys. Rev. Lett.* **125**, 038003 (2020).
- [72] S. Henkes, K. Kostanjevec, J. M. Collinson, R. Sknepnek, and E. Bertin, Dense active matter model of motion patterns in confluent cell monolayers, *Nat. Commun.* **11**, 1405 (2020).
- [73] L. Caprini, U. M. B. Marconi, C. Maggi, M. Paoluzzi, and A. Puglisi, Hidden velocity ordering in dense suspensions of self-propelled disks, *Phys. Rev. Research* **2**, 023321 (2020).
- [74] L. Caprini and U. Marini Bettolo Marconi, Spatial velocity correlations in inertial systems of active brownian particles, *Soft Matter* **17**, 4109 (2021).
- [75] G. Szamel and E. Flenner, Long-ranged velocity correlations in dense systems of self-propelled particles, *EPL (Europhysics Letters)* **133**, 60002 (2021).



# Supplementary Material: Kinetic Monte-Carlo Algorithms for Active-Matter systems

Juliane U. Klamser,<sup>1,\*</sup> Olivier Dauchot,<sup>1,†</sup> and Julien Tailleur<sup>2,‡</sup>

<sup>1</sup>*Gulliver Lab, UMR CNRS 7083, PSL Research University,  
ESPCI Paris 10 rue Vauquelin, 75005 Paris, France*

<sup>2</sup>*Université de Paris, Laboratoire Matière et Systèmes Complexes (MSC), UMR 7057 CNRS, F-75205 Paris, France  
(Dated: December 30, 2021)*

## Contents

<b>I. Numerical implementation in 2d and persistence time</b>	1
A. Numerical implementation of the reflecting boundary condition for the evolution of the self-propulsion speed	1
B. Computation of the persistence time	1
<b>II. Simulation parameters</b>	2
<b>III. AKMC algorithms and persistent time in 1d</b>	3
<b>References</b>	4

## I. NUMERICAL IMPLEMENTATION IN 2D AND PERSISTENCE TIME

### A. Numerical implementation of the reflecting boundary condition for the evolution of the self-propulsion speed

The discrete-time implementation of the velocity dynamics is a random walk with circular reflecting boundaries as illustrated in Fig. S1a. In this random walk, the new velocity  $\mathbf{v}(t_{n+1})$  is sampled from a Gaussian distribution centered at  $\mathbf{v}(t_n)$ , of standard deviation  $\delta v = \sqrt{2D_v dt}$ . The reflecting boundary conditions are implemented as elastic reflections at  $|\mathbf{v}| = v_0$  that are applied when the point sampled by the Gaussian is located outside the circle (see Fig. S1a).

For a free particle, the Metropolis filter in Eq. (1) of the main text is one, *i.e.* every particle displacement is accepted  $\mathbf{r}(t_{n+1}) = \mathbf{r}(t_n) + dt \mathbf{v}(t_n)$ . Fig. S1b shows a discrete-time trajectory where persistent motion is evident.

In the limit of  $dt \rightarrow 0$ , the random walk of  $\mathbf{v}$  converges to the Langevin dynamics (12) in the main text. The corresponding persistence time is computed below, and given in Eq. (5). Figure S1c shows a rapid convergence of the discrete-time algorithm to his asymptotic value for the persistence time.

### B. Computation of the persistence time

In the continuous-time limit, the velocity dynamics is:

$$\dot{\mathbf{v}} = \sqrt{2D_v} \boldsymbol{\zeta}, \quad (1)$$

with reflecting boundary conditions at  $|\mathbf{v}| = v_0$  and  $\boldsymbol{\zeta}$  an uncorrelated unitary Gaussian white noise. To compute the persistence time  $\tau$ , we consider the corresponding diffusion equation in polar coordinates  $(v, \theta)$ ,

$$\partial_t P_t(v, \theta) = D_v \Delta P_t(v, \theta) \quad (2a)$$

\*Electronic address: juliane.klamser@espci.psl.eu

†Electronic address: olivier.dauchot@espci.fr

‡Electronic address: julien.tailleur@u-paris.fr

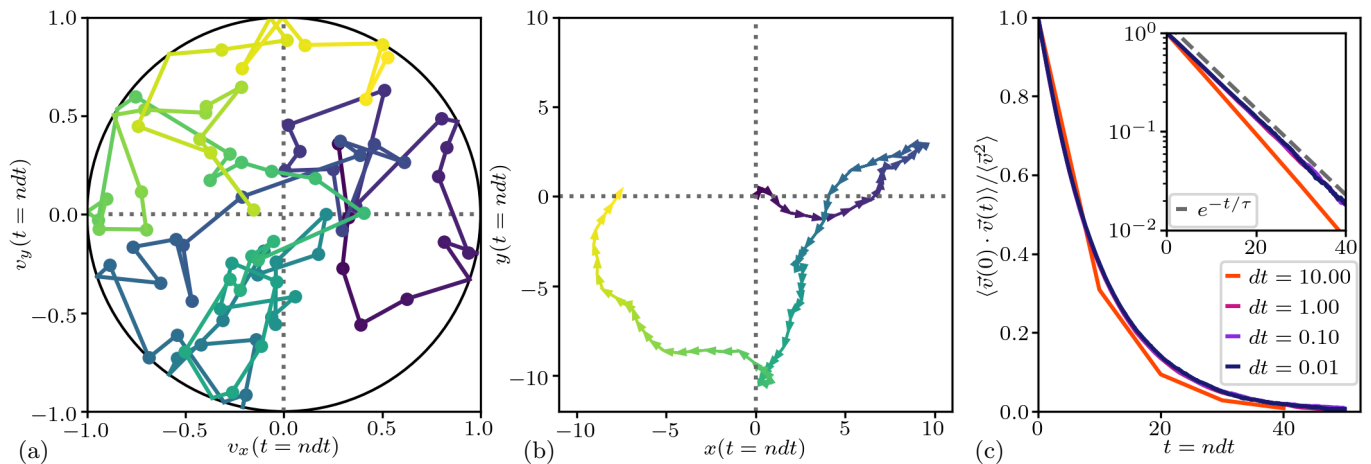


FIG. S1: **(a)** Random walk of  $\mathbf{v}$  in the presence of circular reflecting boundaries at  $|\mathbf{v}| = 1$ ,  $\tau = 10$  and  $dt = 1$ . The symbols correspond to the successive values of  $\mathbf{v}(t_n)$ . The color encodes progress in time from dark to light shades in (a) and (b). **(b)** The particle trajectory in position space corresponding to (a). **(c)** Normalized velocity auto-correlation for the decreasing values of  $dt$  indicated in the legend. Remaining parameters as in (a). Overlapping curves show a fast convergence as  $dt \rightarrow 0$ . The semilogarithmic scale in the inset highlight the validity of the analytical expression (5) for the persistence time.

with a zero current condition at  $v = v_0$ ,

$$\partial_v P_t(v, \theta) |_{v=v_0} = 0. \quad (2b)$$

The corresponding propagator is

$$P_t(v, \theta | v', \theta') = \frac{1}{\pi v_0^2} + \sum_{m=1}^{\infty} \sum_{n=1}^{\infty} e^{-t/\tau_{mn}} J_m \left( \frac{s_{mn}}{v_0} v \right) [A_{mn} \cos(m\theta) + B_{mn} \sin(m\theta)], \quad (3)$$

where  $\tau_{mn} = \frac{v_0^2}{s_{mn}^2 D_v}$ ,  $J_m(x)$  is the  $m^{\text{th}}$  Bessel function of the first kind [1], and  $s_{mn}$  is the  $n$ -th zero of  $\partial_x J_m(x)$ , which follows from the Neumann boundary conditions in Eq. (2b). The constants  $A_{mn}$  and  $B_{mn}$  are functions of the initial velocity  $(v', \theta')$ .

We compute the persistence time from the exponential tail of the velocity autocorrelation in the stationary state

$$\langle \vec{v}_2(t_2) \vec{v}_1(t_1) \rangle = \int_0^{2\pi} d\theta_1 d\theta_2 \int_0^{v_0} dv_1 dv_2 v_1 v_2 \cos(\theta_2 - \theta_1) P_{t_2-t_1}(v_2, \theta_2 | v_1, \theta_1) P_{ss}(v_1, \theta_1), \quad (4)$$

where  $P_{ss}(v_1, \theta_1) = \frac{1}{\pi v_0^2}$  is the uniform stationary distribution. For large  $t_2 - t_1$ , the leading-order contribution comes from the term  $(m, n) \equiv (1, 1)$  in Eq. (3). This gives  $\langle \vec{v}_2(t_2) \vec{v}_1(t_1) \rangle \sim e^{-(t_2-t_1)/\tau}$ , where the auto-correlation time

$$\tau = \tau_{1,1} = \frac{v_0^2}{c^2 D_v}, \quad (5)$$

with  $c \equiv s_{1,1} \simeq 1.841$ .

## II. SIMULATION PARAMETERS

**Fig. 1a:**  $\alpha = 1$ ,  $\beta = 1$ ,  $v_0 = 4$ ,  $D_v = 4.72$ , leading to  $\tau \simeq 1$ .  $N = 2000$  particles were simulated in a box of size  $L_x \times L_y$ , where  $L_y = 35$  and  $L_x = 158.5$ . Periodic boundary conditions are used along the  $y$  axis whereas hard walls are implemented at  $x = -69.5$  and  $x = 89$ . The asymmetric potential is given by  $V(x, y) = 160(x + 0.5)$  for  $x \in [-0.5, 0]$  and  $V(x, y) = 4(20 - x)$  for  $x \in [0, 20]$ .

**Fig. 1b:**  $\alpha = 1$ ,  $\beta = 1$ ,  $v_0 = 1$ ,  $D_v = 1.475 \times 10^{-3}$ , leading to  $\tau \simeq 200$ .  $N = 43904$  particles were simulated in a box of size  $L \times L$ , where  $L = 468$ . Periodic boundary conditions are used along  $x$  and  $y$  axes.

**Fig. 1c:**  $\alpha = 1$ ,  $\beta = 1$ ,  $v_0 = 1$ ,  $D_v = 2.95 \times 10^{-2}$ , leading to  $\tau \simeq 10$ . Periodic boundary conditions are used along the  $y$  axis with  $L_y = 32$ . The particles are confined along the  $x$  axis at  $x = \pm 64$  by potentials  $U_w(x, y) = \frac{10}{8}(x \pm 64)^8$  for  $|x| > 64$ .

**Fig. 2a:**  $\alpha = 0.4$ ,  $\beta = 1$ ,  $D = 1$ ,  $v_0 = 4$ ,  $D_v = 4.72$  leading to  $\tau \simeq 1$ .  $N = 2000$  particles were simulated in a box of size  $L_x \times L_y$ , where  $L_y = 35$  and  $L_x = 158.5$ . Periodic boundary conditions are used along the  $y$  axis whereas hard walls are implemented at  $x = -69.5$  and  $x = 89$ . The asymmetric obstacle is modelled by a potential  $V(x, y) = 18(x + 0.5)$  for  $x \in [-0.5, 0]$  and  $V(x, y) = 0.45(20 - x)$  for  $x \in [0, 20]$ .

**Fig. 2b:**  $\alpha = 0.6$ ,  $\beta = 1$ ,  $D = 0.05$ ,  $v_0 = 1$ ,  $D_v = 1.475 \times 10^{-3}$  so that  $\tau \simeq 200$ .  $N = 43\,904$  particles were simulated in a box of size  $L \times L$ , where  $L = 270$ . Periodic boundary conditions were used along  $x$  and  $y$  axes.

**Fig. 2c:**  $\alpha = 0.6$ ,  $\beta = 1$ ,  $D = 0.05$ ,  $v_0 = 1$ ,  $D_v = 2.95 \times 10^{-2}$  so that  $\tau \simeq 10$ . Periodic boundary conditions are used along the  $y$  axis with  $L_y = 32$ . The particles are confined along the  $x$  axis at  $x = \pm 64$  by potentials  $U_w(x, y) = \frac{10}{8}(x \pm 64)^8$  for  $|x| > 64$ .

**Fig. 3a:**  $\beta = 1$ ,  $D = 1$ ,  $v_0 = 1$ ,  $D_v = 8.1055 \times 10^{-2}$  so that  $\tau \simeq 5$ ,  $dt = 10^{-4}$ . The confining potential is given by  $U_w(x, y) = \frac{\Omega}{\nu}(x \pm 15)^\nu$  for  $|x| > 15$  and the different data sets correspond to

- $U_1 : \nu = 8, \Omega = 10$ ,
- $U_2 : \nu = 6, \Omega = 10$ ,
- $U_3 : \nu = 4, \Omega = 10$ ,
- $U_4 : \nu = 2, \Omega = 100$ ,
- $U_5 : \nu = 2, \Omega = 10$ .

**Fig. 3b:**  $\beta = 1$ ,  $\hat{D} = 1/6$ ,  $v_0 = 1$ ,  $D_v = 8.1055 \times 10^{-2}$  so that  $\tau \simeq 5$ ,  $dt = 10^{-4}$ . The confining potential is given by  $U_w(x, y) = \frac{\Omega}{\nu}(x \pm 5)^\nu$  for  $|x| > 5$ , with  $(\nu, \Omega)$  as in Fig. 3a.

### III. AKMC ALGORITHMS AND PERSISTENT TIME IN 1D

We describe below the one-dimensional version of the blended AKMC; the purely active AKMC that we initially describe in the Letter corresponds to setting  $\alpha = 1$  in the text below.

In 1d, an isolated particle of position  $x$  and velocity  $v$  in the presence of an external potential  $U(x)$  evolves as follows. In one MC step, the particle attempts a move  $x_n \rightarrow x_n + \Delta x$ . With probability  $\alpha$  the displacement is active, i.e.  $\Delta x = dt v_n / \alpha$ , and with probability  $1 - \alpha$  the particle attempts a passive move, i.e.  $\Delta x = \xi$ , with  $\xi$  uniformly sampled in  $[-\sqrt{6Ddt}/(1 - \alpha), \sqrt{6Ddt}/(1 - \alpha)]$ . In both cases, the move is accepted with a probability given by the Metropolis filter  $f(x_n, \Delta x) = \min[1, \exp(-\beta\{U(x_n + \Delta x) - U(x_n)\})]$ . A new velocity  $v_{n+1}$  is then sampled. As in 2d, the velocity undergoes a random walk with reflecting boundary conditions at  $|v| = v_0$ . The new velocity  $v_{n+1}$  is sampled from a Gaussian distribution centred at  $v_n$  and of standard deviation  $\delta v = \sqrt{2D_v dt}$ . When the resulting value  $\hat{v}$  is outside the interval  $[-v_0, v_0]$ ,  $v_{n+1}$  is obtained using the elastic reflection at  $|v| = v_0$ :

$$v_{n+1} = \begin{cases} q - v_0, & \text{if } q < 2v_0 \\ 3v_0 - q, & \text{if } q \geq 2v_0 \end{cases}, \quad (6)$$

where  $q = (\hat{v} + v_0) \bmod (4v_0)$ . Here we use the definition of the modulo as  $a \bmod b = a - b \lfloor \frac{a}{b} \rfloor$  with  $\lfloor a \rfloor$  denoting the floor function. Therefore,  $q$  satisfies  $0 \leq q < 4v_0$  and thus  $|v_{n+1}| < v_0$ .

In 1d, the velocity dynamics describing the blended AKMC in the continuous-time limit is given by  $\dot{v} = \sqrt{2D_v} \zeta$ , with additional reflecting boundaries at  $|v| = v_0$ , and  $\zeta$  is again a unitary Gaussian white noise.

The derivation of the persistence time in 1d is analogous to the 2d calculation, leading to the corresponding propagator

$$P_t(v|v') = \frac{1}{2v_0} + \frac{1}{v_0} \left( \sum_{n=2,4,6}^{\infty} A_n \cos\left(\frac{n\pi v}{2v_0}\right) e^{-t/\tau_n} + \sum_{n=1,3,5}^{\infty} B_n \sin\left(\frac{n\pi v}{2v_0}\right) e^{-t/\tau_n} \right), \quad (7)$$

with

$$\tau_n = \frac{4v_0^2}{n^2\pi^2 D_v}, \quad (8)$$

and the constants  $A_n$  and  $B_n$  are functions of the initial  $v'$ . Following a similar argument as in 2d, the auto-correlation time  $\tau \equiv \tau_1$  as given in the Letter.

- 
- [1] M. Abramowitz and I. A. Stegun, *Handbook of Mathematical Functions with Formulas, Graphs, and Mathematical Tables* (Dover, New York, 1964).